Auxiliary Material for EPAPS:

Measurement of intrinsic Dirac fermion cooling on the surface of a topological insulator Bi_2Se_3 using time- and angle-resolved photoemission spectroscopy

Y. H. Wang, D. Hsieh, E. J. Sie, H. Steinberg, D. R. Gardner, Y. S. Lee, P. Jarillo-Herrero and N. Gedik

SI I. Material preparation

Two types of single crystal Bi_2Se_3 samples are prepared which allow us to span the surface doping range investigated in the main text. For the high doping level samples where $E_D = 0.28$ eV below E_F, stoichiometric mixture of Bi and Se are used. And for the low doping level samples where $E_D = 0.06$ eV, the initial mixture of Bi:Se = 2:4.06 are used. E_D in between these two levels are tuned through the surface doping effect of Bi_2Se_3 [Fig. S1] [1]. Bulk carrier density can be estimated from the Fermi energy and effective mass $m^* = 0.13m_e$ [2]. For the high doping sample, it is $3\times10^{19}\text{cm}^{-3}$ and for the low doping sample $3\times10^{18}\text{cm}^{-3}$. ARPES spectra [Fig. S1 (c)] show rigid shift of E_D over time, consistent with the surface doping effect. A typical scan of TrARPES spectra is performed in 20 minutes for one doping level, during which the band-bending effect is negligible [1, 3].

More details about the surface doping effect of Bi_2Se_3, including rigid band-shift as a function of time after cleaving, potential dopants and theoretical model for such effect, can be found in [3] and the references therein.

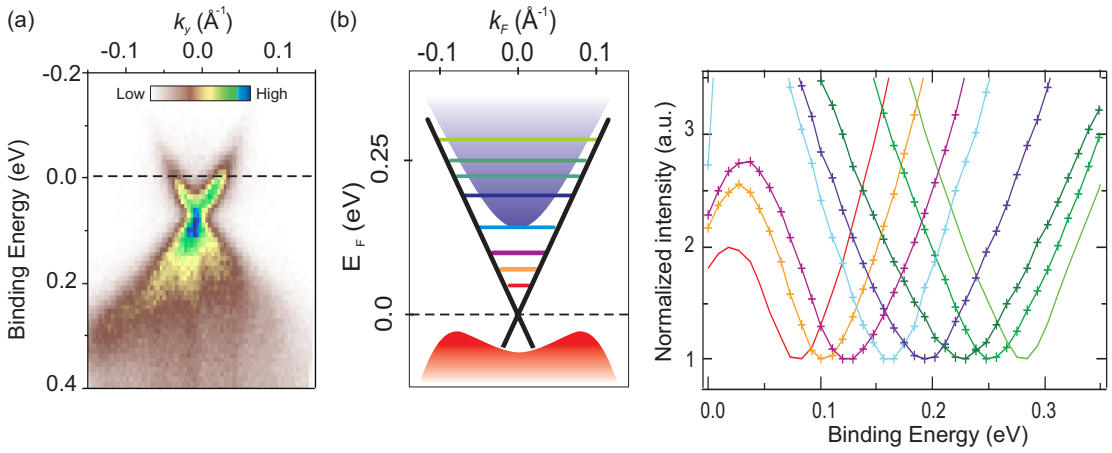

FIG. S1. Bi_2Se_3 surface-doping effect tunes electron density and Fermi level. (a) Energy momentum slice through the $I(E, k_x, k_y)$ spectra for low doping level sample with $E_D = 0.07$ eV above the Dirac point right after cleaving. (b) Momentum integrated spectra showing the shift of the Dirac point due to surface-doping over 24 hours. The Dirac point is lowered from 0.07 eV to 0.28 eV below the Fermi level (traces with markers). Red and green traces without markers correspond to the spectra of high and low doping samples right after cleaving. The intensities are normalized to the intensity at the Dirac point.

SI II. Fitting the TrARPES spectra

In this section, we describe the fitting routine used to obtain the temperature and chemical potential in the main text and show the appropriateness and the uniqueness of the fit and no interdependence among the parameters.

Eq. 1 is a standard equation to describe the momentum-integrated photoemission spectrum that is proportional to the product of the Fermi-Dirac distribution and the density of states (DOS), convolved with a broadening term $G(\epsilon, w)$ [7]. There are four essential fitting parameters at each time point. $A(t)$ is a scaling factor to account for the photocurrent fluctuation and reduced spectral weight in the observed energy-momentum volume after

photoexcitation. $T_e(t)$ and $\mu(t)$ determines the width and the position of the Fermi edge. $w(t)$ is the parameter to account for the energy resolution and spectral broadening due to increased scattering rate after photoexcitation [5]. In general, such broadening might be energy dependent. Here we are only interested in the temperature and chemical potential so we approximate by a constant w for all energy and do not separate the resolution part and broadening part. Note that w is independent of T_e because it is mainly determined by the spectral broadening away from the Fermi level. Such broadening gives rise to the intensity at the Dirac point (E_D) where DOS is zero. $D(E)$ is not a function of t and is chosen to be linear (parabolic) for SS (CB) initially and then iteratively optimized by minimizing χ^2 for all t [4, 5]. $D(E)$ for SS at E_D and $D(E)$ for CB below the conduction band minimum are fixed to be 0. $D(E)$ typically converges in less than four iterations.

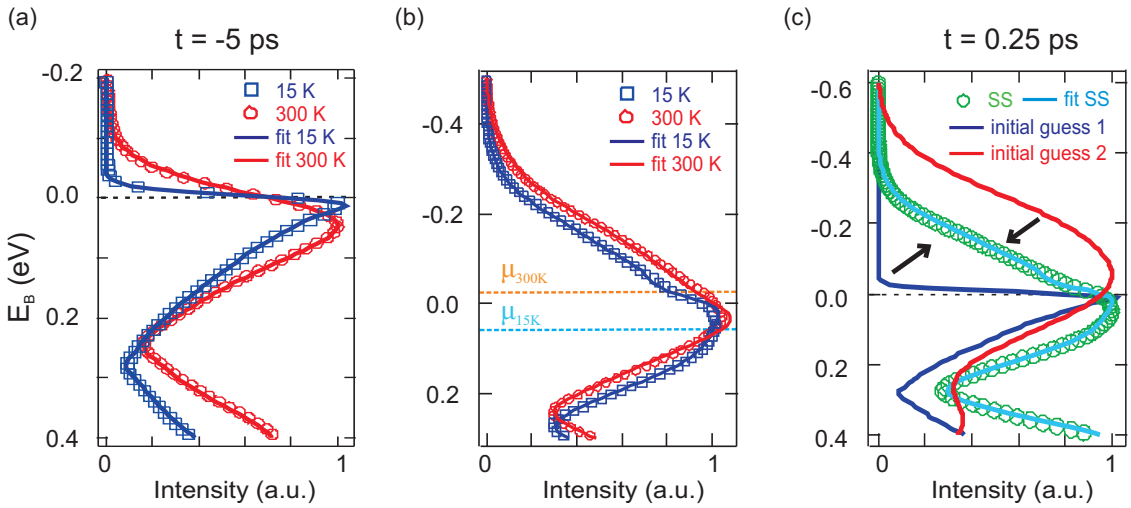

FIG. S2. TrARPES spectra and fit at different t. (a) is the data (markers) and fit (lines) at t = -5 ps. (b) shows the spectra of SS at 0.25 ps and CB at 0.75 ps. (c) shows the $t = 0.25$ ps spectra of SS. The purple and the red traces show the completely different initial guesses used to obtain the best fit (cyan).

	(a) 15 K	(a) 300 K	(b) 15 K	(b) 300 K
T_e	18.3 ± 4.5 K	289 ± 1.6 K	1006.5 ± 3.2 K	1056.3 ± 6.2 K
E_F	-1 ± 0.01 meV	4 ± 0.4 meV	61.1 ± 1.8 meV	-23.2 ± 2.5 meV
w	14.9 ± 4.6 meV	24.2 ± 1.8 meV	40.2 ± 2.2 meV	29.1 ± 1.9 meV

To further prove that the parameters are not interdependent, we show two different fits of the SS spectra at 15 K and 300 K before [Fig. S2(a)] and after [Fig. S2(b)] photoexci-

tation. The delay times in (b) are 0.25 ps for SS and 0.75 ps for CB, when their electronic temperatures are roughly the same. It is chosen because their chemical potentials can be compared directly [Fig. S2(b) dashed lines]. The parameters yielded by the fittings are tabulated below. We can see that the obtained electronic temperatures in (a) are very close to the lattice temperatures which are 20 times different; whereas the values of E_F are similar and clearly do not depend on the values of T_e. On the other hand, the temperatures in (b) are similar because they are mostly determined by the excitation laser fluence; whereas the difference in chemical potentials captures the clear shift in the leading edge in [Fig. S2(b)].

In Fig. S2(c), we show two different sets of initial guesses we use for obtaining the fits. The best fits always converge to the same set of parameters regardless of the distinctively different initial parameters used, suggesting that the best fits do not locate in a local minimum and therefore the solution is unique.

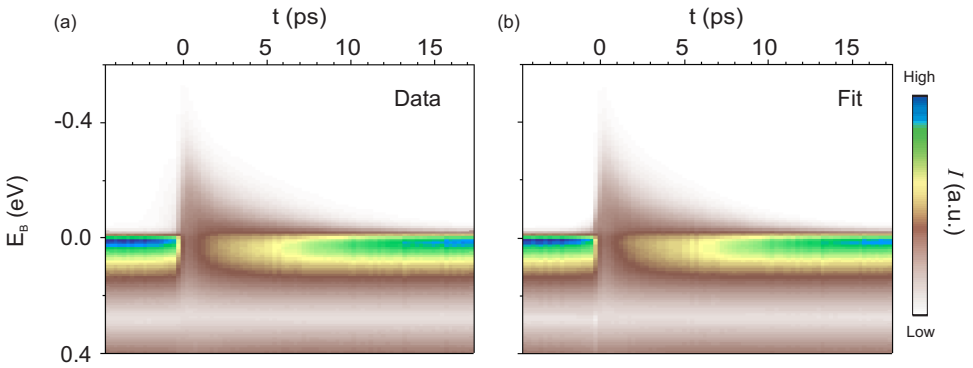

FIG. S3. Agreement between data and fit of the momentum integrated intensity spectra. (a) and (b) show the color map of the data and fit spectra with SS and CB spectra combined. The data is obtained for $E_D = 0.28$ eV sample at 15 K and the fit is performed on the same data set.

The fits are obtained for both SS and CB momentum integrated intensity spectra [Fig. S2(a)] and summed to get the total intensity spectrum at each t point. They are then merged together into a time-resolved intensity spectra as shown in Fig. S3(b). We can see that the fit looks almost identical to the data except in the region -2 ps $< t <$ 0, when the 6.2 eV probe pulse precedes the 1.55 eV pump pulse and excites the system into an image-potential state [6].

SI III. Particle number as a function of temperature and chemical potential

In a static ARPES experiment, the chemical potential of the sample and that of the spectrometer are equal [7]. This is not the case after a femtosecond photoexcitation because electrons can be excited into different bands and it takes certain amount of time for them to relax and equilibrate with the reservoir again.

Even when particle number is conserved in the system, the elevated electronic temperature after photoexcitation changes the chemical potential. This can be seen from the following equation that determines the particle number in a band:

$$N = \int_{-\infty}^{\infty} f_{FD}(E, T_e, \mu) DOS(E) dE \tag{1}$$

where N is the particle number; $f_{\text{FD}}(E, T_e, \mu)$ is the Fermi-Dirac distribution at temperature T_e, $DOS(E)$ is the density of states and E is binding energy. Since density of states is usually energy dependent, at a fixed $N = N_0$, when temperature changes the chemical potential has to change to conserve particle number. Using $D(E) \propto E$ for the surface states of a topological insulator and knowing $T_e(t)$ from our experiment, we can derive $\mu_N(t)$ at a fixed N_0. An example is shown in Fig. S4. We note that, this large change of chemical potential is unique to the SS due to its linear dispersion. As for the CB band density of states, we use a square root function [8] which cuts off at the band minimum because of its parabolic dispersion. In the low doping regime where the CB band is not occupied before photo-excitation ($E_D <= 0.15$ eV), $\mu_N(t)$ is fixed at E_F because $N_0 = 0$ [Figs. S4(b) and (d) red dashed traces]. The actual particle number as a function of time can be straightforwardly calculated (up to a scaling factor) by substituting into Eq. (1) the temperature and chemical potential found from Fermi-Dirac distribution in Eq. (1) of the main text.

Figs. S4(b) and (d) show that for $E_D = 0.15$ eV sample μ^{SS} still overlaps with μ_N^{SS} at 15 K but is much higher at 300 K. Furthermore, Figs. S4(a) and (c) show that SS and CB temperatures do not equilibrate at 15 K in the measured time window but do at 300 K. All these features are consistent with the observation of the main text on a high doping sample.

SI IV. Doping dependence at 300 K

Additional doping dependence of the SS temperature decay at 300 K is shown in Fig. S5. We can see that both the fast and slow components are dependent on E_D [Fig. S5(a)]. Furthermore, the cooling rate $1/\tau_2$ at 300 K lies in the middle of the intrinsic cooling rate

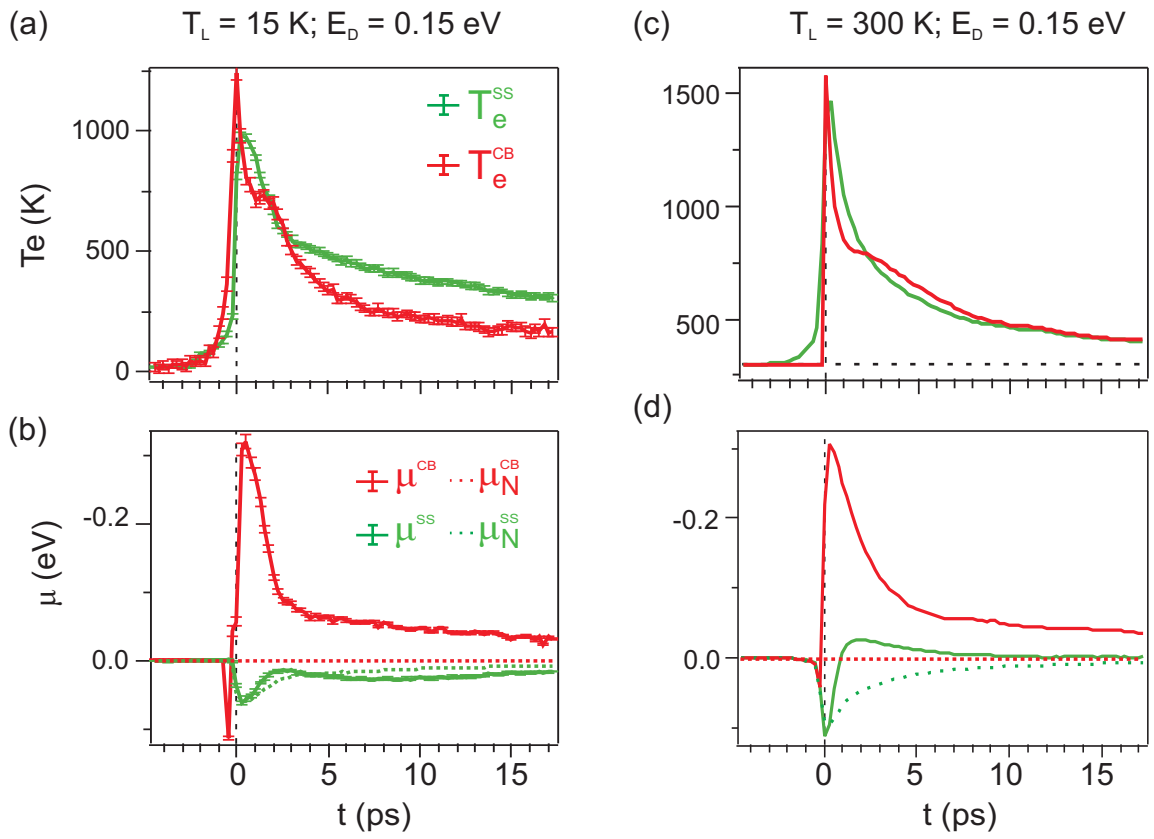

FIG. S4. Electronic temperatures and chemical potentials of SS and CB as a function of t for a sample with $E_D = 0.15$ eV at 15 K ((a), (b)) and 300 K ((c),(d)) lattice temperature. Green traces are for the surface state and red traces are for the conduction bulk band. Green and red dashed traces in (b) and (d) correspond to the chemical potential as a function of its electronic temperature when the particle number is fixed on the surface and conduction bulk band respectively (see text). Error bars of temperatures and chemical potentials from the fitting are shown in (a) and (b). Error bars for other data are similar or smaller.

of SS and CB projected to these doping levels [Fig. S5(b)]. This is consistent with the strong coupling between SS and CB due to interband phonon-scattering. The cooling rate of SS at 300 K is a weighted average of the SS and the CB intraband cooling rate with the weight being the ratio between the intrinsic SS particle number and the particle number transferred from CB to SS via phonon scattering. Since this particle transfer rate depends on the difference between SS and CB chemical potentials, which is a function of E_D, $1/\tau_2$ at 300 K depends on E_D and lies in the middle of $1/\tau_2^{\rm SS}$ and $1/\tau_2^{\rm CB}$.

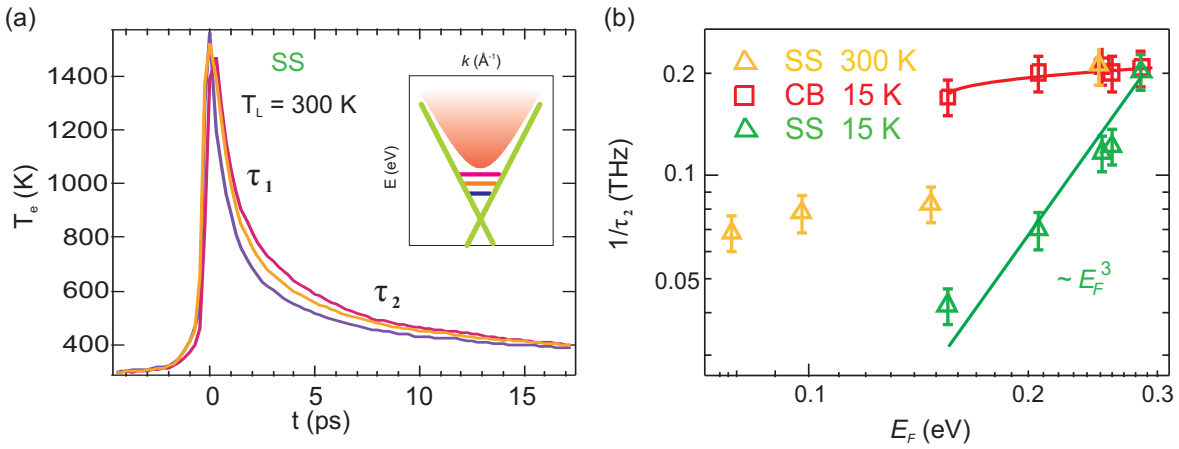

FIG. S5. (a) Doping dependence of electronic temperature of SS at 300 K. The color of the trace matches the color of the Fermi level shown in the inset. Both the fast (τ_1) and slow (τ_2) components are slightly dependent on the doping. (b) $1/\tau_2$ obtained from biexponentially fit the electronic temperature.

[1] Hsieh, et al,. Phys. Rev. Lett. 103, 146401 (2009); Wray et al., Nat. Phys. 7, 32 (2011).

[2] J. G. Analytis, et al., Phys. Rev. B 81, 205407 (2010).

[3] King et al., Phys. Rev. Lett. 107, 096802 (2011); Bianchi et al., Nat. Comm. 1, 128 (2010); Zhu et al., Phys. Rev. Lett. 107, 186405 (2011); Park et al., Phys. Rev. B 81, 041405 (2010).

[4] W. S. Fann, et al., Phys. Rev. Lett. 68, 2834 (1992).

[5] Y. Ishida, et al., Sci. Rep. 1, 64 (2011).

[6] M. Lisowski, et al., Appl. Phys. A 78, 165176 (2004).

[7] S. Hufner, *Photoelectron Spectroscopy* (Springer, Berlin, 2003).

[8] C. Kittel, *Introduction to Solid State Physics*